16th ICAAR LISBOA 2020-2022

16th International Conference on
Alkali-Aggregate Reaction in Concrete
Lisboa | LNEC | Portugal | 31 May - 2 June 2022

http://icaar2020-2022.lnec.pt

Effect of ASR and corrosion on loading capacity and deformation performance of RC beam

Jun Taniguchi [(1)], Yasuhiro Mikata [(2)], Susumu Inoue [(3)]

(1) Kyowa Sekkei Co.,Ltd, Osaka, Japan, taniguchi@kyowask.co.jp

(2) Osaka Institute of Technology, Osaka, Japan, yasuhiro.mikata@oit.ac.jp

(3) Osaka Institute of Technology, Osaka, Japan, susumu.inoue@oit.ac.jp

Abstract

Plenty of researches on alkali silica reaction (ASR) and steel corrosion of RC beam members by unidirectional loading tests have been conducted under various conditions so far. However, these studies have been performed for the purpose of individual material deterioration. For example, the loading capacity of beams, which are affected by ASR tends to increase slightly for that of sound beams due to chemical prestress effect. The most studies have been focusing on the loading capacity of flexure and shear of members. There are very few studies on the flexural stiffness of deteriorated beams and the behavior on postpeak state.

In general, the required performance of a member is considered that the characteristic value until the yield load of the member or the design ultimate load of the member satisfies loading capacity. However, grasping the ductility characteristics from the ultimate load to the failure in design is an important factor in terms of the fail-safe design. Moreover, it is also important to clarify the maximum loading capacity and deformation characteristics of combined deteriorated RC beams due to less research cases.

Based on these backgrounds, this paper takes into account three deterioration factors (steel corrosion, ASR and ASR + steel corrosion) in RC beam members, and the presence or absence of hooks in the axial reinforcing bars in order to evaluate the influence of bond strength reduction due to deterioration. Loading tests for all 34 specimens were conducted and the effects on loading capacity and deformation performance were investigated.

***Keywords**: combined deterioration; loading capacity; deformation performance; RC beam; bond strength*

1. INTRODUCTION

Plenty of researches on alkali silica reaction (ASR) and steel corrosion of RC beam members by unidirectional loading tests have been conducted under various conditions in order to evaluate deteriorations on each material by means of experimental and analytical, and related researches have certainly been accumulated.

However, the most of studies have been focusing on the maximum loading capacity against bending and shear of members in consideration with relationship of cracking conditions, mass decrease ratio of rebars arranged in main direction. Few research cases found regarding bending stiffness and post-peak behaviors.

Based on these backgrounds, this paper intends to evaluate multiple deterioration factors such as steel corrosion, ASR, ASR + steel corrosion and sound condition of RC beam members, and also to evaluate effect of degraded adhesion by deteriorated RC beams using with and without hooks in axial directional rebars. Therefore, unidirectional loading experimental tests to deteriorated RC beams, which were created by a reseach of Mikata et al [1], have been performed to identify the flexural and deformation capacity.

2. OUTLINE OF MATERIALS AND EXPERIMENTS

Figure 2.1 shows the details of the test specimens used in the experiment. Categorized factors are summarized as follows: (1) Type of deterioration: sound specimens (N-series), specimens with ASR (A-series), specimens with corrosion of steel due to salt damage (C-series), specimens with salt damage and ASR (AC-series) were selected. Also, as other categorized factors, (2) Main rebars anchoring part:

Two specimens were prepared, one with a 180-degree hook at the end of the main rebar and the other without hook to evaluate the bond strength between the rebar and concrete. Table 2.1 shows the mixproportion of concrete. D16 ($f_y = 295N/mm^2$) was used for the main rebars, and D6 ($f_y = 345N/mm^2$) was used for the rebars against compression and rebars against shear forces which ratio Pw was set as 0.46%.

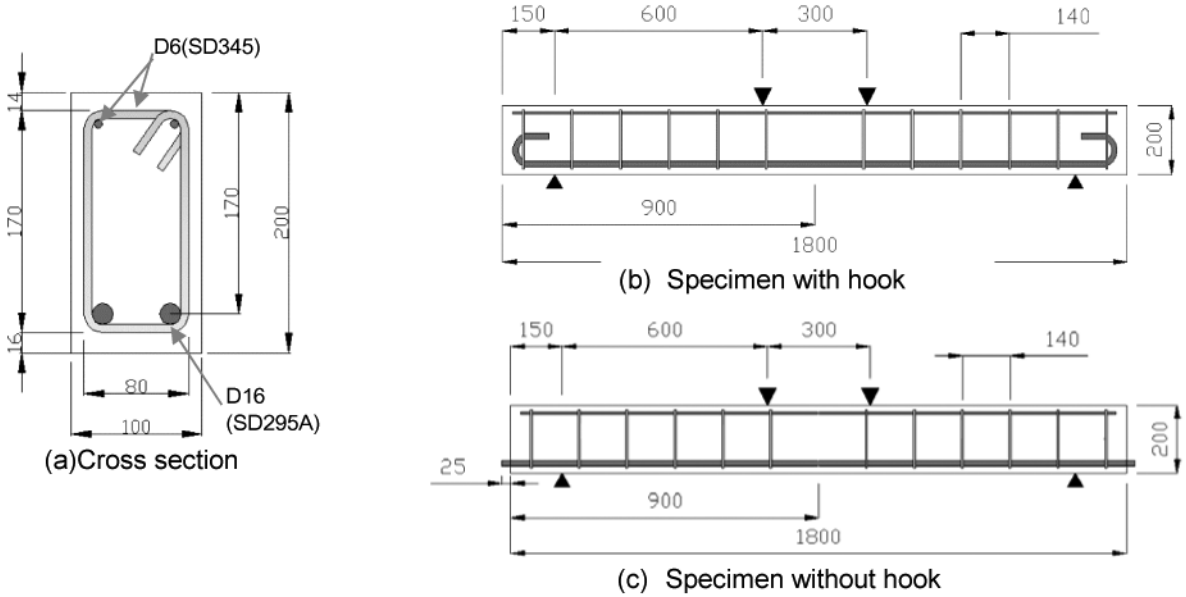

Figure 2.1: Side view and cross-sectional view of the specimen

Table 2.1: Mix proportion of concrete

Series	G_{max}	Slump	W/C	Air	s/a	Unit weight (kg/m^3)							
						W	C	S*1		G*2		NaCl	A*3
	(mm)	(cm)	(%)	(%)	(%)			S_n	S_r	G_n	G_r		(cc)
N	25	8	63	4.0	45.8	183	290	791	0	988	0	0	725
C	25	8	63	4.0	45.8	183	290	791	0	988	0	13.1	725
A, AC	25	8	63	4.0	45.8	183	290	396	411	494	492	13.1	725

*1 S_n : normal fine aggregate, S_r : reactive fine aggregate

*2 G_n : normal coarse aggregate, G_r : reactive coarse aggregate

*3 A : air entraining and water reducing admixture

For A and AC series specimens, in order to create ASR, 13.1 kg / m3 of NaCl, which is equivalent to alkali amount of 7.0 kg / m3 of Na2O, was added. The curing was performed at a temperature of 40 ° C and a relative humidity of 90%. For C-series specimens, 3% concentration of saline water has been sprayed during 5 days a week, and made chloride ions penetrated into the concrete to create salt damage. Table 2.2 shows the curing environment and period of each specimen.

Table 2.2: Curing environment for each specimen

Series	Curing conditions		
	28 days after removal	1st year	2st year
N	Watering curing		
A		Accelerated curing*1	
C		Salt water spray*2	
AC		∗1 ＋∗2	

∗1:Temperature 40 ° C, relative humidity 95%　∗2:Spray 3% salt water 5 times a week indoors

3. EXPERIMENTAL RESULT

3.1 CHEMICAL PRESTRESS

As rebar restrains the concrete expansion caused by ASR reaction, chemical prestress is introduced into the beam specimen. The actual value of expansion was obtained from the strain measured at the rebar, and the analytical value was derived by the equation (1) proposed by Ueda [2] which is expansion prediction model to estimate chemical prestress based on secant rigidity type of constitutive formula using damage theory.

$$\sigma(t) = (1-\Omega)E_{c0} \cdot (\varepsilon_c(t) - \varepsilon_0(t)) \quad (1)$$

where, $\sigma(t)$, $\varepsilon_c(t)$, $\varepsilon_0(t)$: stress on concrete, expansion strain under restrain condition, and expansion strain by ASR without strain condition respectively, with (t) as parameter defined as age of concrete (day). E_{c0}: initial young's modulus of concrete, $\varepsilon_c(t)$: longitudinal free expansion strain of prism specimen by ASR, $\varepsilon_0(t)$: expansion strain at main rebar location for beam specimens. E_{c0} value obtained after 28 days of concrete casting, Ω is a parameter that represents damage and is a monotonically increasing function that is 0 when there is no damage and asymptotes to 1 as damage accumulates. This equation assumes that no damage occurs when the expansion strain is less than the crack initiation strain εcr.

$$\Omega = 0 \qquad \varepsilon_c(t) \leq \varepsilon_{cr} \quad (2)$$

$$\Omega = 1 - \left(\frac{1}{1 + 1000\sqrt{\varepsilon_c(t) - \varepsilon_{cr}}}\right) \qquad \varepsilon_c(t) > \varepsilon_{cr} \quad (3)$$

where, ε_{cr}: strain when initial cracking ($=f_{ct}/E_c$)

Table 3.1: Chemical prestress

Specimens	$\varepsilon_c(t)$ ($\times10^{-6}$)	$\varepsilon_0(t)$ ($\times10^{-6}$)	ε_{cr} ($\times10^{-6}$)	E_{c0} (kN/mm^2)	$\varepsilon_s(t)$ ($\times10^{-6}$)	∗1 E_s(kN/mm^2)	$\sigma(t)$ (mea.) (N/mm^2)	$\sigma(t)$ (cal.) (N/mm^2)
A-F-11	231	2509	46	23.45	309	183.3	3.55	3.66
A-11	349	2509	46	23.45	307	185.3	2.79	2.75
AC-F-11	423	2656	65	25.59	204	181.9	1.82	2.87
AC-11	314	2656	65	25.59	355	178.9	3.12	3.57

∗1 Two corroded main directional rebars were removed from the RC beam after the loading test. The average of elastic modulus was derived by experimental values using the nominal cross-sectional area.

Table 3.1 shows a comparison between actual measured and calculated values of chemical prestress at the main directional rebar position. The free expansion strain ε0 (t) was obtained from the actual measured value of a rectangular specimen (100 × 100 × 400 mm) where no confining rebars were placed which was larger cross section than that of beam specimen (100 × 200 mm), and the water content per unit volume was also larger, accordingly the calculated value of chemical prestress was slightly larger than that of the actual measured value. However, the calculated value of chemical prestress evaluates the measured value precisely.

3.2 MAXIMUM LOAD AND FAILURE TYPE

Table 3.2 shows the calculated flexural capacity and the measured maximum load of the beam specimens, and Figure 3.1 provides the crack state after the loading test. All failure types were flexural tension failure. The flexural capacity was calculated by a fiber model using the actual material strength of concrete and corroded rebars with assumption that degradation of adhesion is not significant. For all specimens, the actual measured maximum load values were larger than those of the calculated values. The reason for this is that the ultimate strain of concrete in the fiber model is 0.0035, which is on the safe side compared to the actual material strain, and chemical prestressing is not taken into account. The material strength of the corroded rebar was obtained by actual tensile test of corroded bar which is removed from specimen after loading test. Regarding cross sectional area of corroded rebar, it was actually difficult to quantify so that the nominal cross-sectional area was used to calculate the yield strength and elastic modulus.Focusing on the cracks before loading, A-08 and A-F-08 specimens were

all cracked by ASR. For the C-08 and C-F-08 specimens, corrosion cracks occurred at the main directional rebars position due to corrosion of those rebars. For the AC-08 and AC-F-08 specimens, in addition to the main directional rebar cracks, ASR cracks occurred on the rebars on compression side. As the main directional rebars restrained the deformation by ASR expansion, it is considered that large number of cracks on upper side observed.

Table 3.2: Results of loading tests

Series	Specimens	Age of concrete (day)	Compressive strength ( ) : 28days stength f'_c (N/mm^2)	The ratio of corrosion weight loss (%)	Ultimate flexural capacity (cal.) P_{ub} (kN)	Ultimate load capacity (mea.) P_u (kN)
N	N-08	28	25.0	-	62.7	76.9
	N-09	28	32.5	-	66.3	74.2
	N-10	28	30.0	-	65.3	75.5
	N-11	28	30.4	-	64.8	73.3
	N-13	28	26.2	-	62.0	70.1
C	C-08	443	28.2	1.6, 2.4	62.5	67.8
	C-09	374	26.7	2.6, 2.7	62.8	72.8
	C-10	377	30.9	1.7, 2.1	65.7	71.8
	C-11	759	24.6	2.2, 1.7	59.8	67.1
A	A-08	761	23.6(31.2)	3.7, 2.8	61.0	75.2
	A-09	368	28.0(23.1)	4.1, 3.7	62.9	73.5
	A-10	740	28.2(27.0)	3.4, 3.1	62.3	64.9
	A-11	757	22.5(16.9)	0.9, 0.9	59.5	67.6
AC	AC-08	761	38.9(28.1)	3.6, 5.4	63.5	65.2
	AC-09	745	30.6(26.4)	3.0, 4.3	63.7	69.8
	AC-10	1134	25.5(26.4)	3.4, 3.2	60.2	66.9
	AC-11	757	21.0(17.9)	3.2, 2.0	56.9	65.7

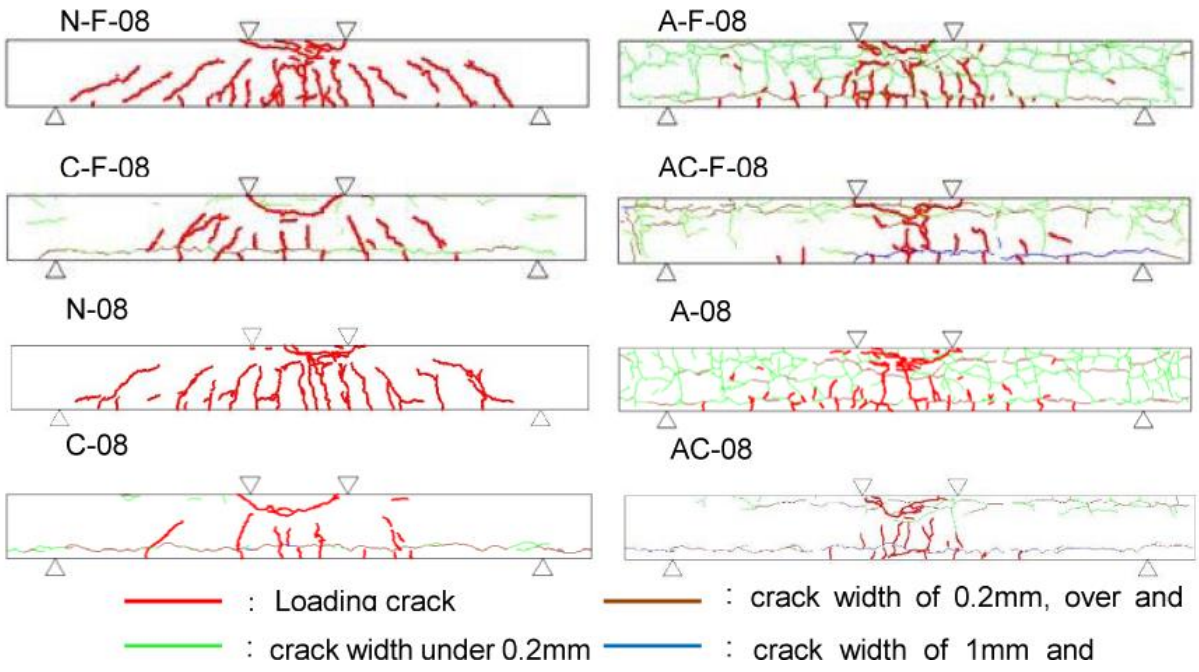

Figure 3.1: Final failure mode

Regarding the cracks during the load, the N-08 and N-F-08 specimens showed shear cracks throughout the shear span where is from the loading point to the support. On the other hand, regarding A-08, AF-08, AC-08, and AC-F-08 specimens, chemical prestress was introduced as rebars restrained ASR expansion so that shear capacity of the specimens were improved, and no shear cracks were confirmed. Focusing on the crack distribution, the distribution was reduced except for the N-series which does not have any cracks even before loading. In particular, for the AC-08 and AC-F-08 specimens, cracks were concentrated only in the flexural span.

3.3 Flexural Capacity of Deteriorated Reinforced Concrete Beams

Figure 3.2 shows the load-center displacement relationship (P-δ) of the test specimens, categorized by the deterioration factors (steel corrosion, ASR, ASR + steel corrosion, soundness) and the presence or absence of hooks on the main rebar.

where P_{max} is the maximum load (KN), δ_{Pmax} is the displacement at the maximum load (mm), the 80% of the maximum load on post peak state was defined as the ultimate load P_e (KN) ($P_{max} \times 0.8$), and δ_e is the displacement at the ultimate load P_e (mm).

Focusing on the maximum load P_{max}, the N and N-F series had the largest value which is about 73KN, and no significant difference was observed with and without the hook. Therefore, from the experimental results, it was confirmed that there was no decrease by bond strength between the sound rebars and concrete. The maximum load of the C, C-F series and the A, A-F series were about the same as around 70KN. The maximum load of the AC and AC-F series had the lowest result as 67KN. Hence, it is considered that the load-carrying capacity was further reduced due to the deterioration caused by steel corrosion in addition to the ASR deterioration.

Next, focusing on the displacement δ_{Pmax} at the maximum load and the displacement δ_e at the ultimate load, the δ_{Pmax} of the N and NF series was about 15mm, and the load increased gently even beyond the yield point which was around 6mm, and the ultimate displacement was around δ_e reached at 22mm which had the highest ductility. The C and C-F series had the maximum load at about 8 mm of displacement near the yield point of the rebars, had no load increase after yielding, had a ultimate displacement of δ_e at about 15 mm, and observed as the largest deterioration in rigidity after yielding compared to the N and NF series. The A, A-F series showed load increase even after yielding then gradually decrease such as load-displacement curve which was not very clear to identify yielding point. δ_{Pmax} and δ_e of A-F series with hook were observed as 2-3mm larger than A series which was without hook. The yield curves of the AC and AC-F series were similar to those of the A and A-F series. The A and AC series are considered due to the improvement of shear strength due to chemical prestress. Compared with the sound specimen, it was confirmed that the maximum load decreased due to ASR deterioration and steel corrosion, the load displacement behavior change after yielding, and the ductility was clearly decreased.

4. ANALYSIS METHOD AND ANALYSIS RESULT

4.1 Analysis Method

In the previous section, the ultimate flexural capacity were calculated by the fiber model using the actual material strengthes, and the results were on the safe values compared to the actual measured values. In this section, the analysis was performed by the three-dimensional nonlinear finite element method, taking into account the fracture energy and tensile softening characteristic as concrete configuration rule, and also the bond slip between the rebars and concrete. The consistency of the experimental results with respect to the stiffness change up to the peak load, post-peak behavior, the state of crack occurrence, and the effects of expansion by ASR and chemical prestress on the RC beam were verified.

The analysis was performed based on the deterioration factors and the main directional rebar shapes i.e. each case (NF-13, N-13, CF-11, C-11, AF-10, A-10, AC-F-10, AC-10) The analysis was applied to total 8 specimens. A symmetrical 1/2 model was used. The solid element was applied for concrete, and the truss element was used for rebars, and the standard element size was set as 25 mm. The concrete compressive stress-strain relationship was set with reference to the research by Saito [3] and Nakamura

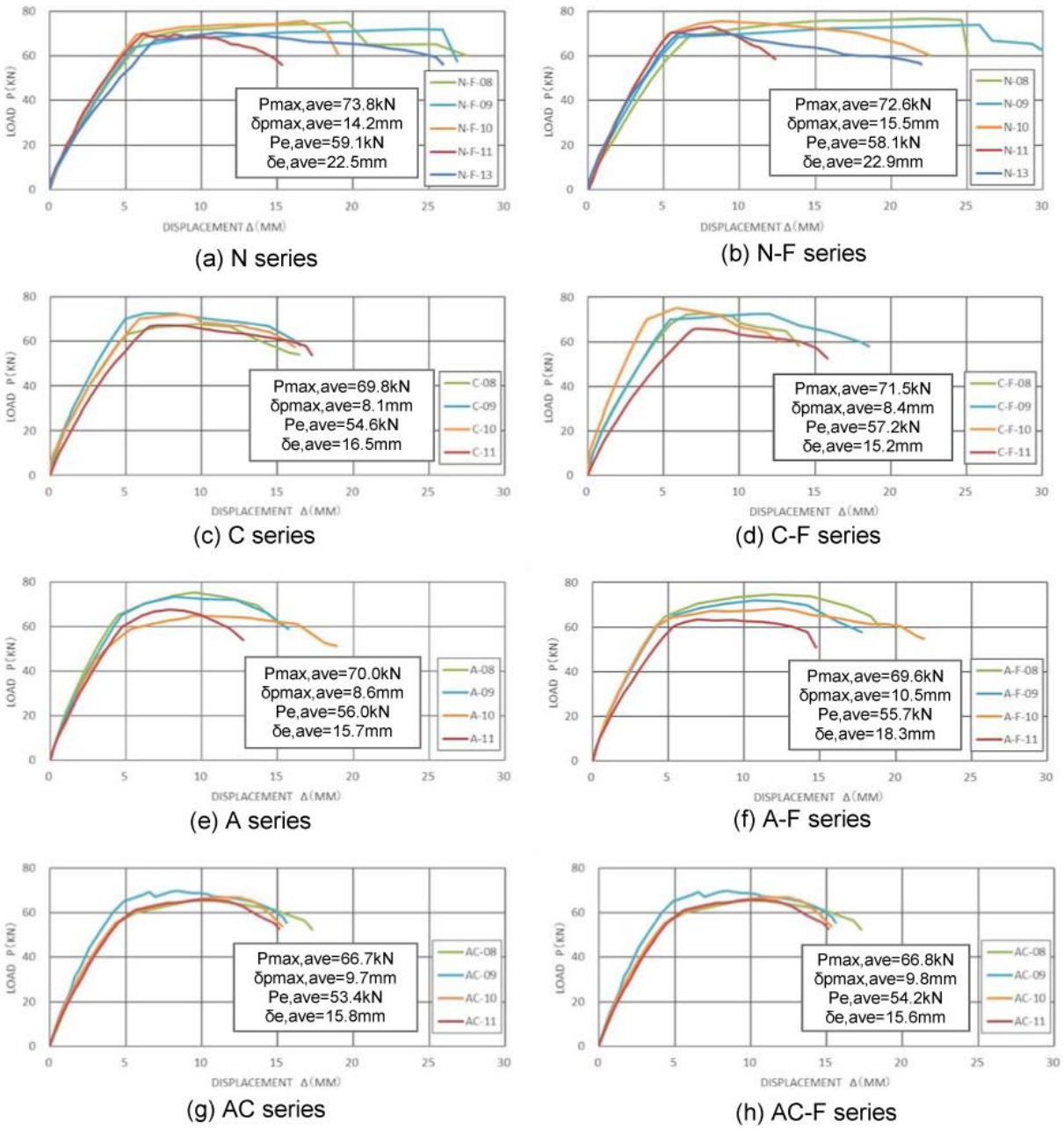

Figure 3.2: Load displacement relationship（mea）

[4]. This model was created in order not to be affected by the element dimensions by dividing G_{fc} by the element height L_{elm}.

$$\sigma = f'_c\left\{\frac{2\varepsilon}{\varepsilon_p} - \left(\frac{\varepsilon}{\varepsilon_p}\right)^2\right\} \qquad 0 \le \varepsilon \le \varepsilon_P$$
$$\sigma = \frac{\varepsilon - \varepsilon_u}{\varepsilon_u - \varepsilon_P} \qquad \varepsilon_p \le \varepsilon \le \varepsilon_u \tag{3}$$

$$\varepsilon_u = \left(\frac{2G_{fc}}{f'_c \cdot L_{elm}} + \frac{\varepsilon_p}{2}\right) \tag{4}$$

$$G_{fc} = 8.8\sqrt{f'_c} \tag{5}$$

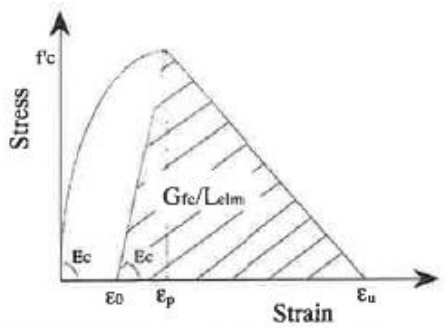

Figure 4.1: Stress-strain relationship of concrete

where G_{fc} is the compressive fracture energy of concrete, f'_c is the compressive strength of concrete (N/mm^2), L_{elm} is the equivalent height of the element (mm), E_c is the Young's modulus of the concrete(N/mm^2), ε_0 is $\frac{\varepsilon_p}{2}$.

For the tensile properties of concrete, the formula (6) specified in the Standard Specifications for Concrete Structures [5] was used.

$$G_F = 10(d_{max})^{1/3} \cdot f'^{1/3}_{ck} \tag{6}$$

where G_F is the tensile fracture energy of concrete, d_{max} is the maximum aggregate size (mm), and f'_{ck} is the compressive strength of concrete (N/mm^2). The stress-strain relationship of the rebar was modelled as bilinear behavior consisting of yield point and tensile strength. Crack model adopted rotary crack model.

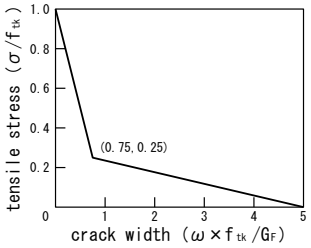

Figure 4.2: Tensile softening curve of concrete

Equations (7) and (8) used for sound concrete proposed by Shima et al. [6] were adopted for the bond stress-slip relationship of the specimens without hook.

$$\tau_S = 0.9f'^{2/3}_c\left(1 - e^{-40S^{0.6}}\right) \tag{7}$$

$$\mathrm{e} = \mathrm{s}/\mathrm{D} \tag{8}$$

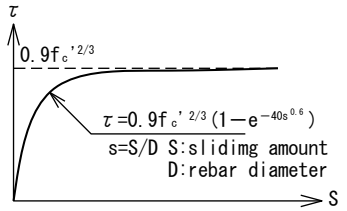

Figure 4.3: Bond stress-slip relationship

where f'_c is the compressive strength of concrete (N/mm^2), S is the amount of slip (mm), and D is the nominal diameter of reinforcing steel (mm). Physical constants such as compressive strength of concrete and tensile strength of reinforcing bars were set based on the results of destructive tests using

the same materials as the specimens. The specimens with hooks at the ends of the main rebars were set to fix the end of reinforcing bar to concrete elements.

As mentioned in the previous section, specimens with degraded ASR (A, A-F, AC, AC-F) are subjected to chemical prestressing because the steel in the specimen restrains the volume expansion caused by ASR. Although the volume expansion due to ASR is anisotropic in nature, the method of isotropic elastic volume expansion by applying a temperature load was adopted because of the high reproducibility of the amount of chemical prestress that mainly affects the maximum load capacity. The introduced temperature was determined by inverse analysis so that the concrete stress near the main directional rebars were equivalent to the stress calculated by equation (1).

The nonlinear solution method was a displacement control type incremental analysis to capture the behavior of post peak state, and the convergence computation was performed by the Newton-Raphson method. Regarding maximum displacement, considering ultimate displacement of each specimen, 25mm for N and N-F series, 15mm for other series respectively, and input mentioned displacement with 50 steps.

Table 4.1: Chemical prestress introduction value

Analysis model	Introduction temperature (℃)	Introduction time (s)	Chemical prestress（N/mm²）	
			Introduced value	Target of introduction value
A-10,A-F-10	9.37	0.1	-5.06	-5.12
AC-10,AC-F-10	11.12		-5.76	-5.59

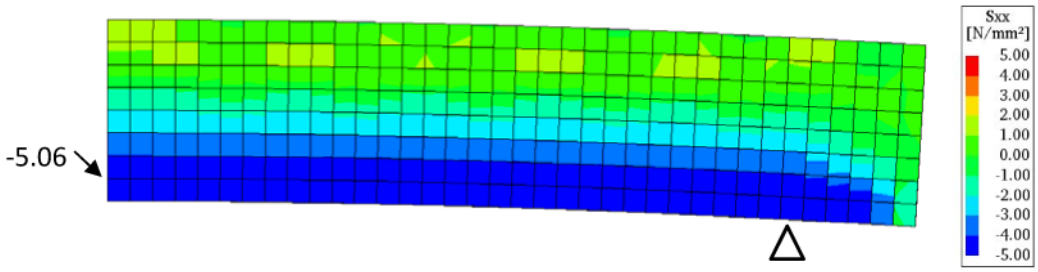

Figure 4.4: ASR expansion analysis

4.2 Analysis Results

Figure 4.5 shows the load-displacement relationship (P-Δ) between the analysis valuess and the measured values, and Figure 4.6 shows the final failure mode of the specimens and the crack strain diagrams at the maximum load. The analysis results for the N series (N-F-13 (analysis), N-13 (analysis)) reproduced almost actual behaviors in both pre-peak and post-peak. The stiffness from the flexural cracking load to the yield load state of the measured value N-13 was slightly higher which is considered as experimental scatter. For the C series, the behavior up to the pre-peak was generally well reproduced. However, while the actual measured value decreased after the yield point, the analytical value slightly increased. The A and AC series were able to reproduce actual behavior both in pre-peak and post-peak. The load-displacement curves with unclear yield points confirmed by actual measurement can also be computed so that the method of introducing chemical prestress by temperature load is a model that can reproduce actual behavior including the increase of shear strength. Focusing on the fracture state of the specimens and the crack strain diagrams at the maximum loads, the crack dispersibility, the occurrence of shear cracks, and the crack direction can be generally reproduced by the analysis. The N series and C series were able to reproduce flexural cracks near the loading point and shear cracks at shear spans. With the A series and the AC series, it was possible to reproduce that there was no shear cracks along with the shear spans by the increase in shear strength due to chemical prestress, also reproduced concentrated flexural cracks near the loading point.

As a general trend comparing the analysis values with the actual measured values, the measured values tended to have slightly higher secondary stiffness from flexural cracking to yielding state. This was due to the fact that in this analysis model, the cross-sectional area was small as 1/6 or less compared to the

main directional rebars (D13), the convergence of the analysis was prioritized, and the rebars on compression side (D6) were not taken into account. The underestimation of compression resistance was considered as one of the factors. Except for the N series, the reason for which the post-peak behavior not well reproduce the actual measured values was considered that the fracture energy calculation formula for sound concrete was applied to the deteriorated concrete.

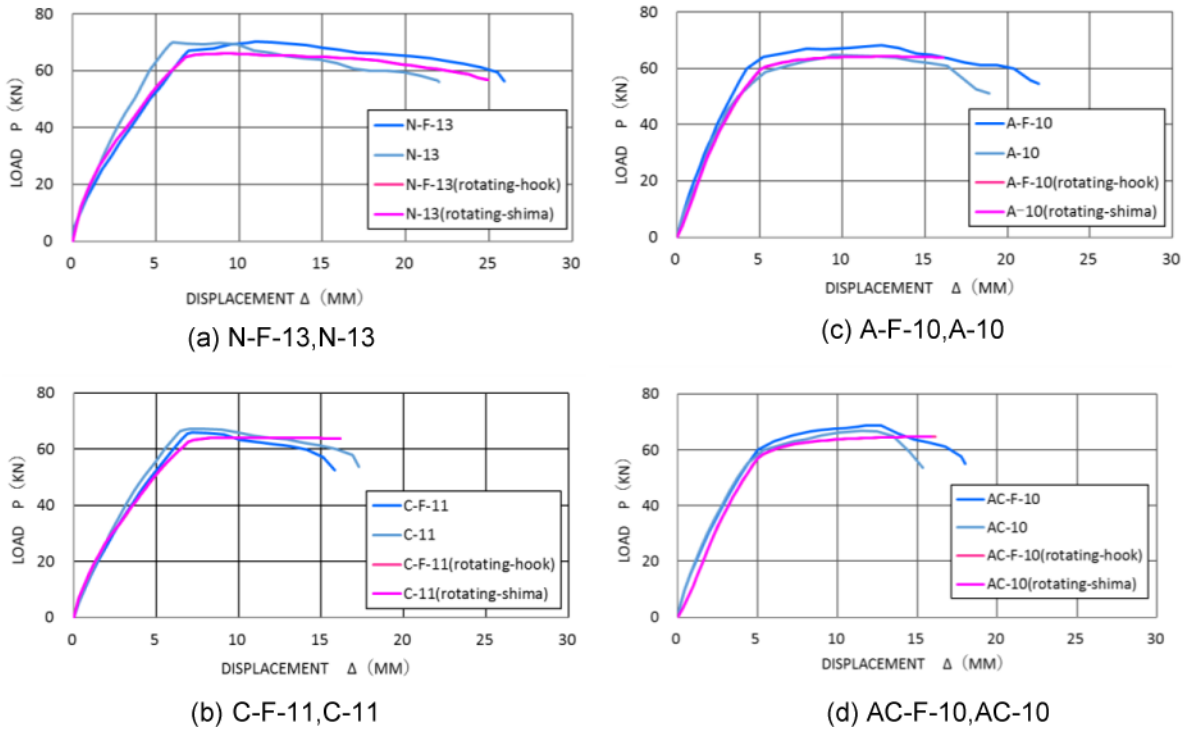

(a) N-F-13,N-13 (c) A-F-10,A-10

(b) C-F-11,C-11 (d) AC-F-10,AC-10

Figure 4.5: Load displacement relationship

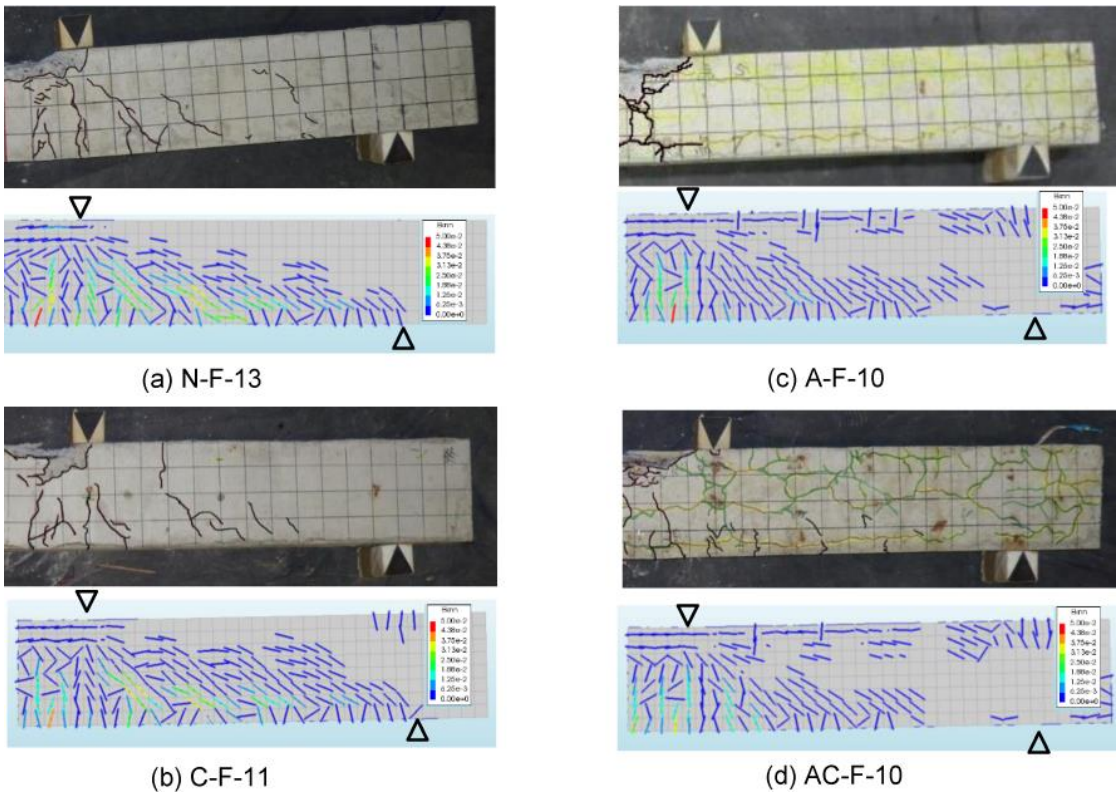

(a) N-F-13 (c) A-F-10

(b) C-F-11 (d) AC-F-10

Figure 4.6: Failure mode and crack strain

In this analysis, the absence of hooks was modelled by bond-slip relationship, and the presence of hooks was modelled as embedded rebar at the end, however no significant difference was found in the load-displacement relationship. From the experimental results, it was confirmed that the deterioration of the bond strength was not remarkable in the degree of deterioration of the specimens, and the analysis also confirmed the same tendency.

5. CONCLUSIONS

The results of loading tests on RC beam specimens with and without axial reinforcing bar hooks were analyzed to evaluate the effects of multiple deterioration factors and the loss of adhesion due to deterioration on load carrying capacity and deformation performance. As a result of the loading tests, the load-center displacement relationship (P-Δ) of the sound specimens (N, N-F) increased slightly after yielding to reach the peak load, and then decreased slowly to reach the final displacement at 20-25 mm. The P-Δ of the corroded steel specimens (C, C-F) showed a peak load at yielding, followed by a decrease in load carrying capacity to reach the final displacement at 15 mm. The P-Δ of the ASR specimens (A, A-F) increased for a while after yielding due to the increase in shear capacity by chemical prestressing, reaching a peak load at about 12 mm and then a final displacement at about 18 mm. The peak load was reached at about 12 mm, and the final displacement was reached at about 18 mm. The P-Δ of the composite degraded specimens (AC and AC-F) was similar to that of the ASR specimens, but the yield stiffness and peak load decreased with steel corrosion compared to the ASR specimens.
Based on the results of the above tests, a three-dimensional nonlinear study was conducted in a limited number of cases, and the findings are summarized below.
(1)As a result of the loading tests, the load of the sound specimens (N, NF) increased slightly after yielding and reached a peak load, then load was decreased on post peak state, and the ultimate displacement was ended up with 20 to 25 mm. After the yield load, P-δ of the steel corrosion test specimen (C,C-F) decreased, and the ultimate displacement ended up with 15 mm. Due to the increase in shear strength by chemical prestress, load of the ASR specimen (A,AC-F) increased for a while after yielding, and reached a peak load at a displacement of about 12 mm, followed by a ultimate displacement of about 18 mm. The P-δ of the combined deteriorated specimens (AC, AC-F) were similar to that of the ASR specimen, but the reduction of the yield stiffness and the decrease of the peak load due to the corrosion of steel were confirmed by compared with the ASR specimen.
(2) It was confirmed that the method adopted in this study was able to generally reproduce actual bhaviors in the pre-peak and post-peak in unidirectional loading of RC beams flexural behavior. In particular, in the case of sound specimens, load-displacement behavior until post peak state was well evaluated. On the other hand, in the test specimens of ASR and ASR + steel corrosion, there was a slight discrepancy of the ultimate strength reduction. This time, the fracture energy was considered in the concrete cofiguration rule, but the proposed formulas of Saito [3] and Nakamura [4] were intended to apply for sound concrete. In the future, it is desired to accumulate data on fracture energy for deteriorated concrete.
(3) The crack condition at the maximum load obtained by the rotating crack model can reproduce actual behavior of the distribution of cracks and the occurrence of shear cracks.
(4) In order to confirm the effect of the presence or bond of hooks at the end of the main rebar by analysis, the specimen without hooks is a model with an adhesion-slip relationship at the boundary between the rebar and concrete, and the specimen with hooks is an embedded rebar. An analysis was performed using a model in which the ends of were fixed, however no significant difference was confirmed. On the other hand, the experimental results confirmed that there was a clear difference in the ultimate displacement between the ASR test specimens with hook and without hook (A-10 and A-F-10), and that the crack dispersibility of the test specimens with hooks was smaller than that of analysis. Therefore, it is necessary to study analysis methods to evaluate these effects further.

6. ACKNOWLEDGMENTS

This work was supported by ABE NIKKO KOGYO Co., Ltd. and JSPS KAKENHI Grant Number JP17K06522.

7. REFERENCES

[1] Effect of Combined Deterioration due to ASR and Corrosion on Loading Capacity of RC Beam, Yasuhiro Mikata, Sho Fukutani, Hideaki Tanaka and Susumu Inoue, International Conference on the Regeneration and Conservation of Concrete Structures, Judged paper, Nagasaki Japan, 2015

[2] Ueda, N, Sawabe, S, Nakamura, H, and Kunieda, M (2007): Numerical study on the expansion induced by alkali silica reaction for RC members, Journal of Japan society of civil engineers, Vol.63 No.4 pp.532-548 (in Japanese)

[3] Saito,S,Nakamura,H,and Higai,T(2001)Analytical study on sliding shear failure of rc panels using rigid-body-spring models, Journal of Japan society of civil engineers, Vol.55 No.704 pp.219-234 (in Japanese)

[4] Nakamura, H, and Higai, T (2001): Compressive Fracture Energy and Fracture Zone Length of Concrete, Modeling of Inelastic Behavior of RC Structures under Seismic Loads, ASCE, pp.471-487

[5] Standard Specifications for Concrete Structures(2012),Jpan,pp38

[6] Shima,H and Yamamoto,K(1991) Local bond stress-slip relation of corroded rebar, Proceedings of the Japan Concrete Institute,13-1 pp663-668